# Lightning Phenomenology Notes

# Note 23

# 8 Jan 2014

# Lightning Responses on a Finite Cylindrical Enclosure

Kenneth C. Chen and Larry K. Warne
Sandia National Laboratories, P. O. Box 5800, Albuquerque, NM 87185, USA
and
Kelvin S. H. Lee
2111 Eric Drive, Los Angeles CA 90049

## Abstract

The voltage on a single –turn loop inside an enclosure characterizes the enclosure shielding effectiveness against a lightning input. In this paper, the maximum induced voltage on a single-turn loop inside an enclosure from lightning coupling to a metal enclosure wall is expressed in terms of two multiplicative factors: (A) the normalized enclosure wall peak penetration ratio (i.e., ratio of the peak interior electric field multiplied by the sheet conductance to the exterior magnetic field) and (B) the DC voltage on an ideal optimum coupling loop assuming the ideal penetration ratio of one. As a result of the decomposition, the variation of the peak penetration ratio (A) for different coupling mechanisms is found to be small; the difference in the maximum voltage hence arises from the DC voltage on the optimum coupling loop (B). Maximum voltages on an optimum coupling loop inside a finite cylinder enclosure for direct attachment, and a lightning line source at different distances from the enclosure are given in Table 3.

## Introduction

Lightning coupling to the enclosure interior can occur in three distinct ways: (1) lightning can attach to the enclosure and the resulting lightning current flowing in the enclosure wall can cause voltage inside the enclosure wall (an attachment); (2) lightning can strike a conductor close to the enclosure (but not the enclosure) and the resulting magnetic flux can induce a voltage inside the enclosure (the distance from the line source to the enclosure can vary theoretically from *0* (closest induction coupling) to some distance (close coupling)); (3) lightning can strike further away from the enclosure (uniform field-drive induction). A finite cylindrical enclosure geometry with end caps is considered a canonical enclosure for aeronautical systems. Reference [1] solves such a canonical problem for a lightning attachment and [2] solves the

general case for the lightning induction coupling by simplifying the enclosure to an infinite flat enclosure wall and provides useful results for the closest induction coupling. References [3] and [4] provide a simple fit function for obtaining the decaying exponential peak responses from two limiting cases (the unit step and impulse peaks) for the closest induction coupling and for a uniform field drive coupling. This paper provides voltage bounds for all these couplings.

The lightning current along the axial direction of the cylinder is considered. In all these couplings, mathematical expressions for the solution of the induced voltages are complicated and not intuitive. However, the maximum voltage on an optimum coupling loop interior to the enclosure can be expressed in terms of two multiplicative factors discussed in the abstract. The benefits of such decomposition are simplicity of the physical interpretation, easy generalization of the result to other coupling configurations, and results free from algebraic errors.

There is a major conceptual difference in the interior voltage for the attachment and induction case. Consider the unit step current that is attached to the enclosure wall. The late-time voltage corresponds to the DC voltage that reflects the effective enclosure resistance driven by the unit step current. For induction, the late-time voltage for a unit step current always decays to zero. We shall artificially derive a DC voltage that corresponds to the concentrated distribution of current in the conductor that exists at the time of peak voltage (The detailed explanation is given in Appendix A).

We study the decomposition in three steps: First, we discuss how the induced voltage for the attachment case [1] is decomposed into two multiplicative factors. Second, we investigate the simplified flat enclosure wall coupling to a lightning line source at an arbitrary distance from the enclosure. Third, the transition from the line source induction coupling to a uniform field drive induction coupling is addressed.

Application to enclosures other than a metal wall is discussed. Enclosures with graphite composite are shown to provide considerably less shielding than enclosures with a metal wall.

# Planar Field Diffusion

One-dimensional magnetic diffusion through a planar slab (with permeability μ and conductivity σ) of thickness Δ is illustrated in Figure 1 and the explicit solution relating the incident decaying magnetic field $H = H_x(0)e^{-\alpha t}u(t)$ to penetrant field $E_z(\Delta, t)$ has been solved in Reference 1 . It is given as

$$\left[\frac{\sigma\Delta E_z}{H_x}\right]\Big|_{pl} = \frac{1}{2\pi i}\int_{r-i\infty}^{r+i\infty}\frac{e^{st}\sqrt{\sigma\mu s}\Delta ds}{(s+\alpha)sinh(\sqrt{\sigma\mu s}\Delta)} = \left[\frac{\sqrt{\alpha\tau_d}}{sin(\sqrt{\alpha\tau_d})}e^{-\alpha t} + 2\sum_{n=1}^{\infty}(-1)^n\frac{(n\pi)^2}{(n\pi)^2-\alpha\tau_d}e^{-\frac{(n\pi)^2}{\tau_d}t}\right] \quad (1)$$

Here the diffusion time $\tau_d = \Delta^2\mu\sigma$. Although (1) consists of an infinite series, the sum represents multiplicative factor A as discussed in the Abstract for specific coupling geometries such as direct attachment and distant coupling. For a unit step ($\alpha \to 0$), (1) becomes

$$\left[\frac{\sigma \Delta E_z}{H_x}\right]\Big]_{pl} = \left\{1 + 2\sum_{n=1}^{\infty}(-1)^n exp\left[-(n\pi)^2 \frac{t}{\tau_d}\right]\right\} \quad (2)$$

An asymptotic form of (2) for early time is

$$\left[\frac{\sigma \Delta E_z}{H_x}\right]\Big]_{pl} \sim 2\sqrt{\frac{\tau_d}{\pi t}} e^{-\frac{\tau_d}{4t}}, \quad (3)$$

which is twice the half-space solution (derived in (B16) for close induction), is more convenient for numerical evaluation for early time.

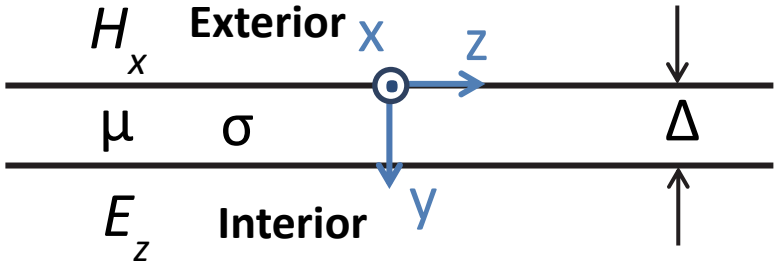


**Figure 1. Flat Enclosure Wall.**

For an impulse ($\alpha \to \infty$),

$$\left[\frac{\sigma \Delta E_z}{H_x}\right]\Big]_{pl} \alpha\tau_d = -\sum_{n=1}^{\infty}(-1)^n 2(n\pi)^2 exp\left(-(n\pi)^2 \frac{t}{\tau_d}\right), \quad (4)$$

which can be obtained by taking the time derivative of (2).

# Induced Voltage for End-to-End Lightning Attachment on a Cylindrical Can

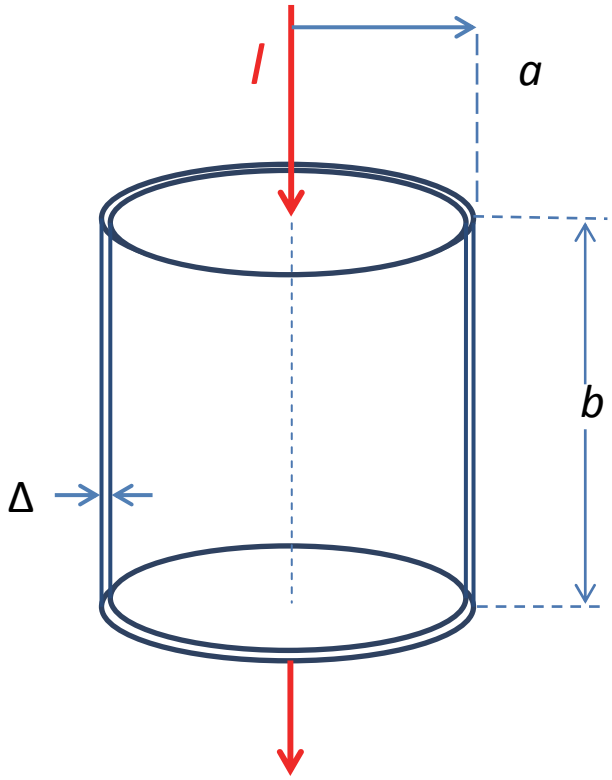


**Figure 2. A symmetrical lightning strike applied to the center of both end caps of a finite cylindrical enclosure.**

The i
caus
be

$$V \approx \frac{I}{2\sigma\Delta\pi}\left[2ln\left(\frac{a}{\Delta e^{-\gamma}}\right)+\frac{b}{a}\right]\left[\frac{\sigma\Delta E_z}{H_x}\right]\Big|_{pl} \quad (5)$$

where $\left[\frac{\sigma\Delta E_z}{H_x}\right]\Big|_{pl}$ given by (1) has been discussed in the previous section and $\gamma \approx 0.5772$. Notethat in (5), the logarithmic term contributes from lightning entering and exiting end caps and $\frac{b}{a}$ contributes from the lightning current flowing axially on the cylindrical surface.

The induced voltage along the center dashed line in Figure 2 from the magnetic flux of the enclosure lightning current is zero because of there is no flux penetration. The right hand side of (1) consists of two multiplicative factors: (A) $\left[\frac{\sigma\Delta E_z}{H_x}\right]\Big|_{pl}$ or (1) that can be interpreted as the planar penetration ratio of the interior electric field to the exterior magnetic field multiplied by the sheet conductance. (B) the second multiplicative factor is the DC voltage that is coupled to an optimum coupling loop.

Note that the only time dependent function is the penetration ratio. Now if we are only interested in the peak in (1), we can approximate the peak as a function of $\alpha\tau_d$ by a fit function to be given next. Peaks of (1) as a function of $\alpha\tau_d$ (peak penetration ratio) are plotted against a fit function based on peaks of unit step and impulse responses, (2) and (4), in Figure 3.

Previously [3], [4], an approximate technique for calculating peak exponential response from the unit step and impulse peaks for magnetic field and line source coupling has been introduced. Treating the unit step and impulse components as independent because the unit step peak contributes to the low frequencies and the impulse peak to high frequencies, a parallel "combination" of unit step coupling and the impulse coupling for the attachment case gives

$$\frac{1}{P_p^{de}} \approx \left(\frac{1}{P_p^s} + \frac{1}{P_p^i}\right), \tag{6}$$

which is shown as "approximation" in Figure 3 and where $P_p^{de}$, $P_p^s$ and $P_p^i$ are the uniform field drive peak penetration ratio for a decaying exponential (1), a unit step (2) and an impulse (4), respectively.

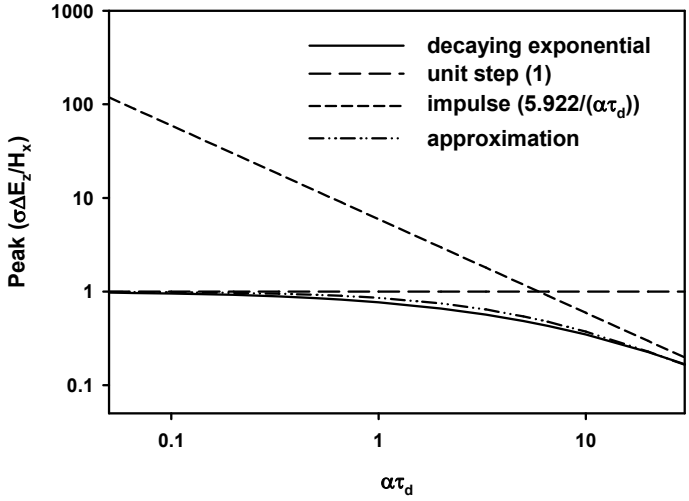


**Figure 3. Peak voltage bound for Planar Penetration.**

Note that the superscript "de", "s" and "i" denote decaying exponential, step and impulse, respectively; the subscript "p" denotes the planar or uniform field drive.

For a single-loop voltage bound, the worst-case coupling can be approached (the distance between the line source and the flat plate is theoretically assumed to be zero) when lightning strikes a well-insulated cable that is isolated from the enclosure, but their separation is sufficient to withstand the high potential. For the worst-case coupling, the cable that is struck by lightning is shown in Figure 4.

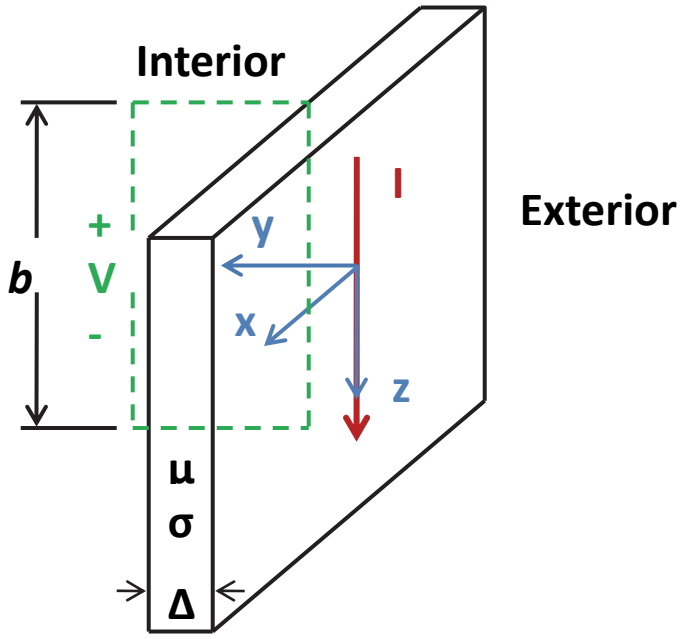


**Figure 4. Direct lightning strike to an insulated cable parallel to (and adjacent to) the enclosure wall and a maximum coupling loop.**

Defining peak penetration ratios as in (6), the peak voltage as shown in Figure 4 can be expressed as [3], [4]

$$Peak\ V \approx \frac{I}{\sigma\Delta}\left(\frac{b}{\pi\Delta}\right) P_c^{de}\ ; \qquad \frac{1}{P_c^{de}} = \frac{1}{P_c^{s}} + \frac{1}{P_c^{i}} \tag{7}$$

where $P_c^{de}$ , $P_c^{s}$ and $P_c^{i}$ are the peak penetration ratios for the closest induction case. Peak penetration ratios normalized by π are plotted in Figure 5 for a decaying exponential, a unit step and an impulse, respectively. Note that the superscript "de", "s" and "i" denote decaying exponential, step and impulse, respectively; the subscript "c" denotes the closest induction.

Finally, the artificial DC voltage (the decomposition factor (B)) ♠ on an optimum coupling loop $\frac{I}{\sigma\Delta}\left(\frac{b}{\pi\Delta}\right)$ assuming the penetration ratio is one.

## Line Source at a Distance

We observe that the planar peak penetration ratio for lightning attachment and the closest line source induction peak penetration ratio as shown in Figure 3 and Figure 5 ($P_c$ is normalized by π) are not far apart numerically. The planar penetration should be applicable to the case where $d \gg \Delta$. In the attachment case, the voltage appears on the enclosure wall interior; while the line source induces a voltage on an optimum coupling loop or equivalently on the enclosure wall interior (This is the maximum voltage that can arc to an insulated wire adjacent to the enclosure wall.)

♠ This voltage appears on a uniform enclosure wall conductor of length *b* and cross-section area $\pi\Delta^2$.

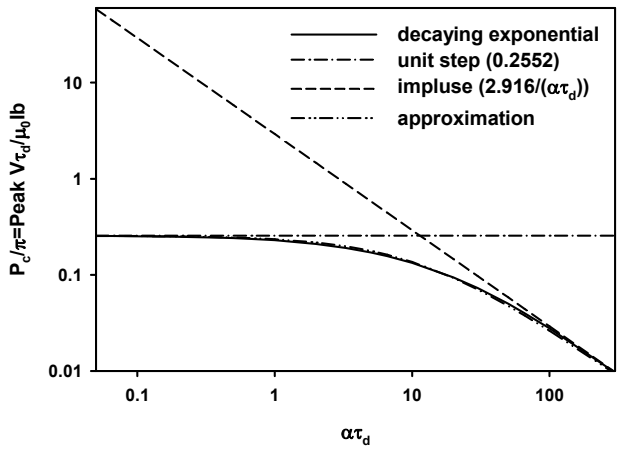


**Figure 5. Peak voltage bound for direct strikes.**

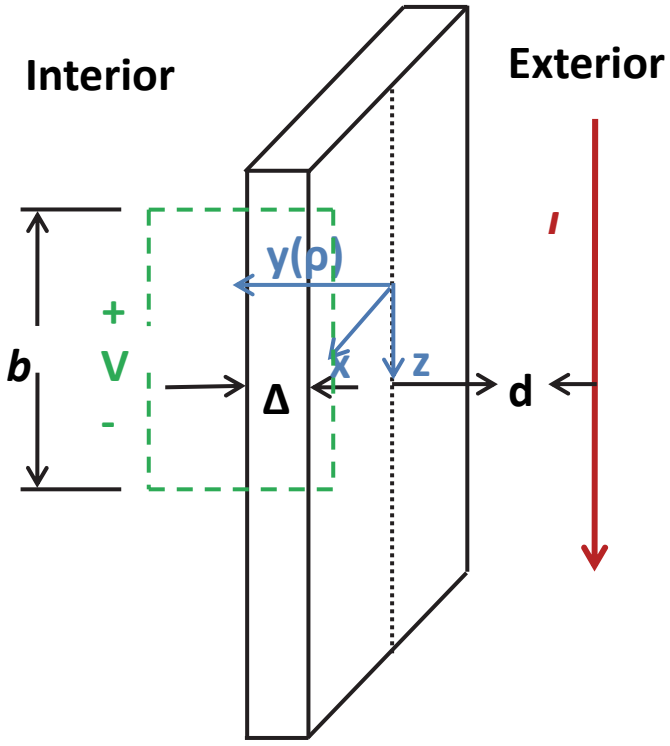


**Figure 6. Direct lightning strike to an insulated cable parallel to and *d* distance away from the enclosure wall.**

As shown in Figure 6, the optimum coupling voltage from a line source in the *z*- direction at a distance *d* from the flat enclosure wall can be expressed as

$$V \approx \frac{1}{\sigma\Delta}\left[\frac{\Delta\sigma E_z}{H_x}\right]\Big|_{pl} \frac{I2b}{2\pi d} \approx \frac{I}{\sigma\Delta}\left[\frac{\Delta\sigma E_z}{H_x}\right]\Big|_{pl} \frac{b}{\pi d} \qquad (8)$$

In the middle expression of (8), the incident magnetic field is $\frac{I}{2\pi d}$ at the enclosure exterior surface and a factor of 2 in the numerator is due to the image. The ideal coupling factor for

very close induction is now $\frac{b}{\pi d}$. A uniformly valid coupling coefficient for the induction case can be taken as $\frac{b}{\pi(d+\Delta)}$, which avoids the singularity as $d \to 0$ and gives the right limiting value. Therefore, (8) is modified to

$$V \approx \frac{I}{\sigma\Delta}\left[\frac{\Delta\sigma E_z}{H_x}\right]\Big|_{pl} \frac{b}{\pi(d+\Delta)} \tag{9}$$

Note that we use the planar penetration ratio that is derived from the attachment case. In the induction case, as $t \to \infty$, $V \to 0$. This will be rigorously derived in Appendix A and B. Specifically, the exact residue series for the penetration ratio for a unit step drive is derived in (A17) and the early-time expansion that shows $V \to 0$ as $t \to \infty$ is given in (B16). Since only the peak fit function is used in applications, the waveform issue is not important.

# Enclosure Magnetic Field Penetrations

When lightning return stroke location is far away from the enclosure, the nearby lightning magnetic field is used as the incident field excitation. The maximum induced voltage on an optimum coupling loop can be expressed in terms of the two multiplicative factors. We proceed to derive these two factors for this case. The peak time derivative of the magnetic field inside the enclosure is (Figure 7)

$$Peak\ \frac{dH_{in}^{e}}{dt} \approx \frac{H_{ext}}{\xi\tau_d} p_f^{de};\ \xi = \frac{\mu_0 V}{\mu S\Delta}\ ; p_f^{de} \approx \frac{1}{\frac{1}{0.8876}+\frac{\alpha\tau_d}{5.7118}} \tag{10}$$

where the factor $p_f^{de}$ that was calculated in [4] is now defined as the enclosure penetration for a uniform field drive. The subscript "*f*" denotes the field drive. For a non-magnetic enclosure case and a circular cylinder, $\xi \approx \frac{a}{2\Delta}$.
We will show that, for the peak induced voltage on an optimum coupling loop,

$$V = \mu_0 Peak\ \frac{dH_{in}^{e}}{dt} 2ab \tag{11}$$

can be expressed in terms of these two multiplicative factors.

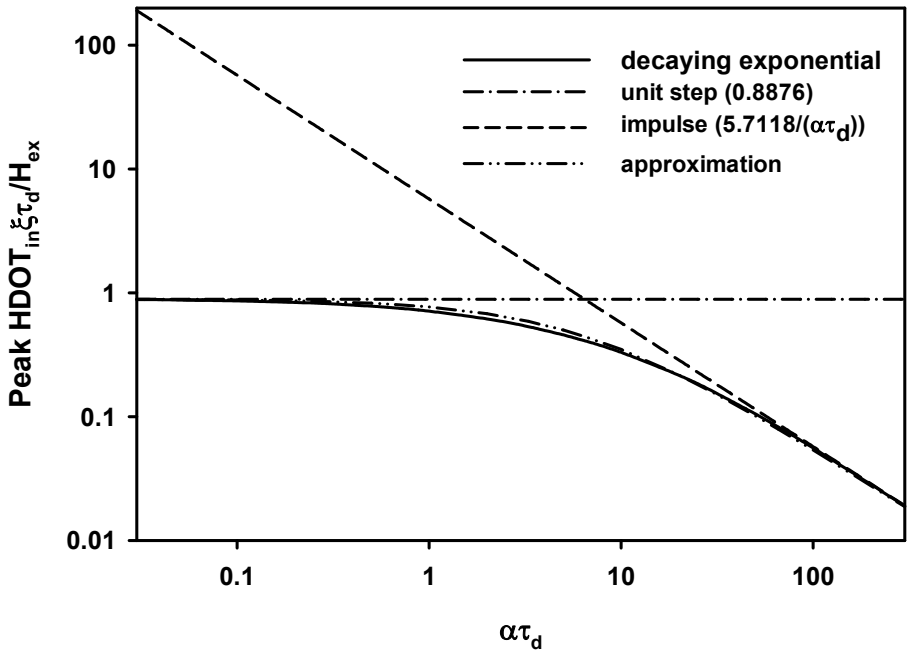


**Figure 7. Penetration Ratios for a Field Drive. Note that $HDOT = {dH}/{dt}$.**

## Transition from a Line Source to a Uniform Magnetic Field Drive

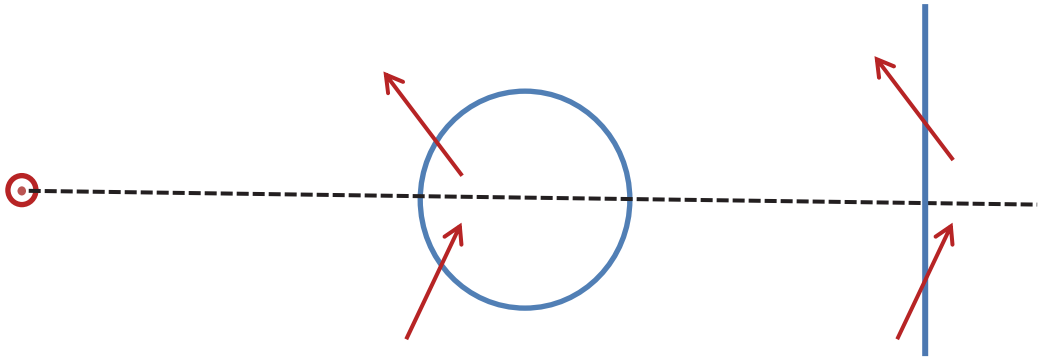

**Figure 8. Magnetic flux from a line source pointing out of the paper is shown as red arrows penetrating the enclosure wall.**

The idealized flat enclosure wall coupling configuration discussed (Figure 6) is accurate when the distance between the lightning current and the enclosure wall (*d*) is small compared to the enclosure dimension. The magnetic flux coupling from the line source to a flat enclosure wall model is shown (on the right of Figure 8) and to the enclosure (in the middle of Figure 8). The magnetic flux coupling from a uniform field drive to a cylindrical enclosure is shown in Figure 9. The line source model does not include the enclosure late-time decay feature described by the

inductance and resistance of the enclosure equivalent circuit as discussed in [5], [6], [7], [4] and therefore the peak voltage on an optimum coupling loop for a slender cylindrical enclosure is a factor of two lower. The transverse magnetic field coupling to the cylinder is treated because it optimizes the voltage coupling.

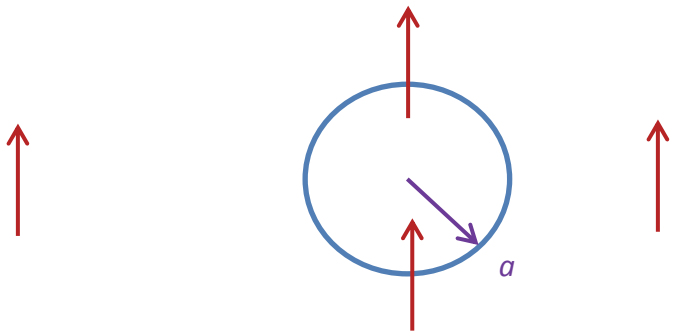


**Figure 9. Magnetic flux from a uniform field drive is shown as red arrows penetrating the enclosure wall.**

For large *d*, the magnetic flux shown in Figure 9 should be used to drive the enclosure and the more accurate voltage is thus attained from a uniform field drive model.

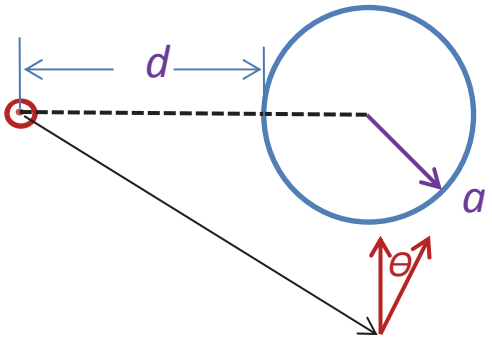


**Figure 10. A approximate transition between the line source model and the uniform drive model is $d = \sqrt{2}a$.**

The uniform field drive assumes that the magnetic field is uniform (i.e.,$d \gg a$, where *a* is the enclosure dimension shown in Figure 9); the line source flat enclosure wall model is applicable to $d \ll a$. The difference in the voltage calculated for the example of a finite cylindrical enclosure geometry using the line source flat enclosure model is off by less than a factor of *2* for $d \to \infty$. A possible dividing line is illustrated in Figure 10: use the flat wall model for $d \leq \sqrt{2}a$ and use the uniform field drive for $d > \sqrt{2}a$. At $d = \sqrt{2}a$, the component of the magnetic field perpendicular to the enclosure is assumed to be a uniform drive of the enclosure that gives the same DC voltage factor (A) on an optimum coupling loop as the line source. The

penetration ratio for the line flat enclosure model can differ from that for a uniform field drive model by 10% (**Table 1**).

The magnetic field component normal to a cylindrical enclosure in Figure 10 is given by

$$H_{ext} = \frac{I}{2\pi}\frac{d+a}{(d+a)^2+a^2} \tag{12}$$

and thus the peak induced voltage is

$$V = \frac{I}{\sigma\Delta}\frac{2b(d+a)}{\pi[(d+a)^2+a^2]}p_f^{de}, \tag{13}$$

which is decomposed into two factors: the penetration ratio $p_f^{de}$ and the remaining multiplicative factor on the right hand side of (13) (the DC voltage). In concluding this discussion, the voltage bound for $0 \le d \le \sqrt{2}a$ is described by (9) and the voltage bound for $\sqrt{2}a < d$ is described by (13).

# Numerical Comparisons

The planar penetration ratio is based on penetration through one flat enclosure plate; the field drive enclosure penetration ratio is based on penetration through one enclosure plate with the presence of another flat plate at an enclosure dimension distance [5]. Their numerical values are not very far apart. Apart from the application of a planar penetration ratio to the attachment case, the penetration ratio for coupling from an adjacent closest line source, to a line source at a distance, and finally to a uniform field drive can cover the whole range of transition from near field to far field. **Table 1** documents numerical penetration ratio peaks for closest line coupling (after normalization by *1/π*), for the planar case (applicable to the intermediate distance and the enclosure lightning attachment), and for a uniform field drive as a function of decaying exponential parameter $\alpha\tau_d$.

**Table 1**. Comparison of Actual Voltage Peaks (Penetration Ratios) and Their Approximations for Closest Line Source, Planar Line Source Far Field), and Uniform Field Drive (Enclosure Penetration) Diffusions.

| $\alpha\tau_d$ value | Closest Induction Penetration Ratio $P_c^{de}$ | Approximate Closest Induction Penetration Ratio $1/\left(\frac{1}{P_c^s}+\frac{1}{P_c^i}\right)$ Percentage deviation (%) | Planar Penetration Ratio $P_p^{de}$ | Approximate Planar Penetration Ratio $1/\left(\frac{1}{P_p^s}+\frac{1}{P_p^i}\right)$ Percentage deviation (%) | Penetration Ratio Accounting for enclosure geometry | |
|---|---|---|---|---|---|---|
| | | | | | Enclosure Penetration ratio $P_f^{de}$ | Approximate Enclosure Penetration ratio $1/\left(\frac{1}{P_f^s}+\frac{1}{P_f^i}\right)$ Percentage deviation (%) |
| 0.05 | 0.797 | 0.7983 (0.16%) | 0.9732 | 0.9916 (1.89%) | 0.873 | 0.8808 (0.89%) |

| | | | | | | |
|---|---|---|---|---|---|---|
| 0.066 | 0.7955 | 0.797 (0.19%) | 0.9666 | 0.9889 (2.31%) | 0.8688 | 0.8786 (1.13%) |
| 0.1 | 0.7923 | 0.7948 (0.32%) | 0.9536 | 0.9834 (3.13%) | 0.8602 | 0.874 (1.6%) |
| 0.2 | 0.7829 | 0.7879 (0.64%) | 0.922 | 0.9673 (4.91%) | 0.8371 | 0.8608 (2.83%) |
| 0.33 | 0.7713 | 0.7791 (1%) | 0.8876 | 0.94729 (6.71%) | 0.8103 | 0.8443 (4.2%) |
| 0.5 | 0.7571 | 0.7681 (1.45%) | 0.8507 | 0.9221 (8.39%) | 0.7805 | 0.8236 (5.52%) |
| 0.66 | 0.7449 | 0.7581 (1.77%) | 0.8211 | 0.8997 (9.57%) | 0.7562 | 0.805 (6.45%) |
| 1 | 0.7201 | 0.7373 (2.39%) | 0.7686 | 0.8855 (15.2%) | 0.7111 | 0.7682 (8%) |
| 2 | 0.6594 | 0.6824 (3.49%) | 0.6598 | 0.7475 (13.27%) | 0.6155 | 0.6771 (10%) |
| 3.3 | 0.5985 | 0.622 (3.93%) | 0.567 | 0.6421 (13.25%) | 0.5325 | 0.5867 (10%) |
| 5 | 0.5372 | 0.5576 (3.8%) | 0.485 | 0.5422 (11.79%) | 0.4575 | 0.4995 (9.18%) |
| 6.6 | 0.4917 | 0.5083 (3.38%) | 0.4292 | 0.4729 (10.2%) | 0.4061 | 0.4382 (7.9%) |
| 10 | 0.4191 | 0.4276 (2.03%) | 0.3475 | 0.3719 (7%) | 0.3304 | 0.3475 (5.18%) |
| 20 | 0.2956 | 0.2915 (-1.4%) | 0.2257 | 0.2285 (1.24%) | 0.2157 | 0.2161 (-0.064%) |
| 30 | 0.229 | 0.2212 (-3.41) | 0.1673 | 0.1649 (-1.43%) | 0.1603 | 0.1568 (-2.18%) |

Table **1** also provides the comparison between the approximate fit functions versus the actual peaks previously shown in Figure 3, Figure 5 and Figure 7. The percentage deviation of the approximation from the actual numerical value is given in parenthesis in the entries for approximate ratios. Because of the assumption that the unit step peak contributes independently of the impulse peak the maximal deviation occurs near $\alpha\tau_d \sim 3.3$. Notice the difference between the planar penetration ratio and the enclosure penetration ratio for a uniform field drive is approximately 10% for the thin enclosure thickness limit and negligible for the thick enclosure limit. The planar penetration ratio is approximately 24.7% greater than the closest induction penetration ratio for a unit step excitation ($\alpha\tau_d = 0$), while the planar penetration ratio is approximately 35% less than the closest induction penetration ratio for an impulse excitation ($\alpha\tau_d = \infty$) (Figure 3 and Figure 5). The crossover point appears to be ($\alpha\tau_d \approx 2$) (**Table 1**).

Time-domain voltage waveforms for the closest induction penetration and the planar penetration were given in [4] and [1], respectively. Time-derivative waveforms of the magnetic field inside an enclosure (which are identical to the voltage waveforms) are also discussed in [4]. The peak voltage for the impulse closest induction penetration occurs approximately at $t = 0.069\tau_d$; both peak voltages for the impulse planar penetration [1] and the enclosure penetration [4] occur approximately at $t = 0.09\tau_d$. We can assume the time for the flat plate penetration peak increases from $t = 0.069\tau_d$ to $t = 0.09\tau_d$ as *d* varies from *0* to $\sqrt{2}a$. As discussed before, for the unit step case, the peak for the attachment case occurs $t \to \infty$. For the unit step closest induction penetration, the peak occurs at $t = 0.215\tau_d$. For the unit step enclosure uniform field penetration, the peak of the time-derivative of the magnetic field [4] (or its penetration function) occurs approximately at $t \approx 0.5\tau_d$. We surmise that the time corresponding to the peak occurrence of the unit step induction coupling for the flat plate penetration should also increase from $t = 0.215\tau_d$ to $t \approx 0.5\tau_d$ as *d* varies from *0* to $\sqrt{2}a$.

From extensive numerical calculations given in [4], the impulse peak penetration time can be used to approximate the peak penetration time for exponential decay excitation waveforms

with $\alpha\tau_d$ approximately given by the intersection (Figure 5 and Figure 7) of the unit step penetration ratio and the impulse penetration ratio. The unit step peak penetration time can be used when $\alpha\tau_d$ is small.

Table 2 gives an equivalent DC voltage induced on an optimum coupling loop normalized by $\frac{I}{\sigma\Delta}$

**Table 2. Ideal Coupling Factors (Optimum coupling loop DC voltage normalized by $\frac{I}{\sigma\Delta}$) for Lightning Attachment versus Lightning Induction.**

| A Cylindrical Enclosure Dimension | | | Ideal Coupling Factor | |
|---|---|---|---|---|
| Length (*b in*) | Thickness (*Δ in*) | Radius (*a in*) | Attachment to the Center both End Caps $\frac{1}{2\pi}\left(2ln\left(\frac{a}{\Delta e^{-\gamma}}\right)+\frac{b}{a}\right)$ | Closest Induction $b/(\pi\Delta)$ |
| *72* | *1/2* | *6* | *2.885* | *45.837* |
| | | *12* | *2.15* | |
| | | *18* | *1.961* | |
| | *1/8* | *6* | *3.326* | *183.347* |
| | | *12* | *2.592* | |
| | | *18* | *2.402* | |

(the ideal coupling coefficient) for the specific lightning attachment to the enclosure geometry shown in Figure 2 and that for the lightning striking on an adjacent insulated cable as shown in Figure 4. The ideal coupling coefficient for close induction is $\frac{b}{\pi(d+\Delta)}$ rather than $\frac{b}{\pi\Delta}$ for the closest induction case. As a numerical example, when lightning strikes a cable at a distance of approximately *10.16 in* from the closest enclosure wall and the enclosure is *6 ft* in length, *2 ft* in diameter and *½ in* in the enclosure thickness, the maximum voltages received by a single-turn optimum coupling loop are approximately the same as those for the attachment case.

# Maximum Coupling Voltages for Typical Enclosures

A useful enclosure example of aerospace systems is a cylindrical 6061 aluminum alloy enclosure (with end caps) of 6 ft in length, with possible radii of *6 in*, *12 in* and *18* in, and an enclosure thickness of ½ in or *1/8 in*. (
Table 2). The decomposition allows us to determine the maximum voltage on an optimum coupling loop for a worst-case direct strike, for the closest magnetic coupling from a line source insulated from the enclosure, and for a line source at any distance from the enclosure. In order to maximize the voltage coupling, the line source is assumed to be parallel to the cylindrical axis of the enclosure. As a worst-case calculation, the lightning peak return stroke of *200 kA* is used. The other relevant parameter is the decay constant α of the return stroke, where we use the *1%* charge transfer of the return stroke of *40C* [4] to give $\alpha = 3466\ s^{-1}$.

The approximate fit functions for penetration ratios are adequate for most applications. We can obtain more accurate penetration ratios by using **Table 1**. The conductivity for a 6061 aluminum alloy enclosure case is $\sigma = 2.6 \times 10^7 S/m$ so that, for a ½ in thickness, $\alpha\tau_d \approx 18.37$.

The corresponding $\alpha\tau_d$ is approximately $1.142$ for an enclosure thickness of *1/8 in*. The approximate planar penetration ratio for $\alpha\tau_d = 18.37$ is $0.2436$ and for $\alpha\tau_d = 1.142$ is $0.8383$. Using the difference between the numerical and approximate planar penetration for $\alpha\tau_d = 20$ and $\alpha\tau_d = 1$ for correction, the more accurate planar penetration ratios are *0.2408* for $\alpha\tau_d = 18.37$ and *0.7214* for $\alpha\tau_d = 1$, respectively. The approximate uniform field drive penetration ratios are *0.2303* for $\alpha\tau_d = 18.37$ and *0.7538* for $\alpha\tau_d = 1.142$, respectively. After following a similar correction procedure, the more accurate uniform field drive penetration functions are *0.2299* for $\alpha\tau_d = 18.37$ and 0.6967 for $\alpha\tau_d = 1.142$, respectively.

Notice the difference between the planar penetration ratio and the uniform field drive penetration ratio for the same $\alpha\tau_d$ are less than 10%. Assuming a *1%* lightning peak current of $I = 2 \times 10^5\ A$, the normalizing sheet factors (voltage) are $\frac{I}{\sigma\Delta} = 0.6057\ V$ for $\Delta \approx {}^{1}/_{2}\ in$ and $\frac{I}{\sigma\Delta} = 2.423\ V$ for $\Delta \approx {}^{1}/_{8}\ in$, respectively. For $d \geq \sqrt{2}a$, a magnetic field drive coupling model is used to calculate the peak maximum coupling voltage (10).

The results can now be summarized in Table 3. The maximum voltages on a gap of the center wire of a finite cylinder are less than *0.5V* for a ½-in enclosure thickness and are approximately less than *6V* for a 1/8-in enclosure thickness, respectively, for lightning attaching to the center of the end caps. Moving on to the next column, we can verify easily (by setting $d = 0$ in the formula) that the closest coupling maximum voltages are approximately *8.57V* for the ½-in case and *324V* for the 1/8-in case, respectively [4]. The linear extrapolation function given in the footnote and the formulas in the relevant entries of Table 3 allow an estimate of maximum voltages from a line source adjacent to the enclosure to a line source up to a distance $d = \sqrt{2}a$. For $d \geq \sqrt{2}a$, formulas including field drive penetration ratios are used to cover the remaining range. The slight discontinuity of 10% is introduced because of the difference in the planar penetration ratio versus the field drive penetration ratio at $d = \sqrt{2}a$.

**Table 3. Maximum Voltages for Different Coupling Configurations.**

| Cylindrical Enclosure Dimension ( in) | | | Maximum Voltage on an Optimum Coupling Loop (V) | | |
|---|---|---|---|---|---|
| Length (*b*) | Thickness (Δ) | Radius (*a*) | Attachment to the Center of both End Caps | Line Source ($d + a$) from the axis of the cylinder (*d* and *a* in meters); *d* and *a* are defined in Figure 10 | |
| | | | | $d \leq \sqrt{2}a$ | $d \geq \sqrt{2}a$ |
| *72* | *1/2* | *6* | *0.4024* | $\frac{0.3528p^{de^*}}{1.27 \times 10^{-2} + d}$ | $\frac{0.7056p_f^{de}(d+a)}{(d+a)^2 + a^2}$ |
| | | *12* | *0.3* | | |
| | | *18* | *0.274* | | |
| | *1/8* | *6* | *6.075* | $\frac{1.41p^{de^*}}{3.2 \times 10^{-3} + d}$ | $\frac{2.82p_f^{de}(d+a)}{(d+a)^2 + a^2}$ |
| | | *12* | *4.734* | | |
| | | *18* | *4.387* | | |

$^{*}p^{de}(d) = \left[P_c^{de}\left(\sqrt{2}a - d\right) + P_p^{de}d\right]/\left(\sqrt{2}a\right)$

# Graphite Composite Panel

Graphite composite materials have been used for aircraft and other aeronautical systems. The low conductivity value of the graphite composite causes a significant reduction in shielding

effectiveness. A typical graphite composite panel has a thickness on the order of *3 mm* (*1/8 in*) and the conductivity of the composite along the panel is typically $1 \times 10^4\ S/m$. The penetration ratios obtained from the metallic layer are applicable to this case. The peak voltage inside the enclosure is inversely proportional to the conductivity of the enclosure case and the peak voltage of a composite enclosure is thus more than three orders of magnitude greater than that for an aluminum enclosure of identical dimensions.

Assuming a thickness of *3 mm* of composite panel, the diffusion time is $\tau_d = 0.113\ \mu s$. The aluminum conductivity is $3.5 \times 10^7 S/m$, an aluminum foil of *2 mils* thickness has the same diffusion time. Note that the only major difference in the multiplicative factors for the voltage induced on an optimum coupling loop (B) is the scaling factor (the DC square sheet Factor). The composite has a DC square sheet resistance of $\frac{1}{\sigma\Delta} \approx 33\ m\Omega$; the aluminum foil has a DC square sheet resistance of $0.56\ m\Omega$. Therefore, aluminum foils provides considerably more shielding than a much thicker composite panel.

# Conclusions

Interior voltage bounds on a single-turn optimum coupling loop inside a metallic enclosure for various coupling configurations are expressed in terms of two multiplicative factors: (A) the penetration ratio of interior electric field to the exterior magnetic field multiplied by the sheet conductance and (B) the DC voltage that is coupled to the optimum coupling loop when the penetration ratio is one. The lightning coupling configurations include (1) direct attachment and (2) a lightning strike on an insulated cable immediately adjacent to the enclosure; (3) a lightning strike at any distance from the enclosure. Although the methodology is applicable to enclosures of a general shape, we limit the numerical example to a representative aerospace enclosure of a finite cylinder with end caps.

The line source coupling to a flat enclosure wall is used as a canonical problem for describing very close coupling and used to describe the transition to a uniform field drive enclosure model. Therefore coupling configuration (3) is subdivided into (a) a close-in coupling model and (b) a uniform field drive model.

The voltage bound for an optimum coupling loop is calculated for all these coupling configurations so that it is possible to determine the necessary enclosure thickness and material conductivity to mitigate the lightning diffusion insult.

## Appendix A. Rigorous Treatment of Line Source at Distance from the Enclosure

For a direct-strike coupling, the maximum internal fields and pin-level voltages are induced when the lightning channel is inclined at an acute angle with respect to the enclosure wall or for a direct strike to an insulated conductor that is parallel and at a distance *d* close to the outer surface of the wall (Figure 6).

Consider the problem of calculating the transverse magnetic fields on the opposite side of an electrically thick wall (of thickness Δ) due to a parallel current filament with time dependence $i(t) = I\,e^{-\alpha t}u(t)$. According to Reference 2, the exact magnetic vector potential in the transformed domain is

$$A_z^{tot} = \frac{\mu_0 I}{2\pi}\int_0^\infty \frac{(\xi/\nu)e^{\zeta\left(\frac{\Delta}{2}+y-d\right)}cos(\zeta x)}{[\zeta cosh(\xi\Delta/2)+(\xi/\nu)sinh(\xi\Delta/2)][\zeta sinh(\xi\Delta/2)+(\xi/\nu)cosh(\xi\Delta/2)]}\frac{1}{(s+\alpha)}d\zeta \qquad \text{(A1)}$$

where $\nu = \mu/\mu_0$ and $\xi = \sqrt{\zeta^2 - i\omega\mu\sigma} = \sqrt{\zeta^2 + s\mu\sigma}$.

The early-time integral used for obtaining results given in Figure 5 is not used here because we are interested in deriving the penetration ratio valid for any value of *d*. Note that the solution (2), valid for $d \to \infty$, already exists in residue series. The early-time integral is discussed in Appendix B.

The voltage induced on an optimum coupling loop is given by [2]

$$V = b\frac{d}{dt}\frac{1}{2\pi i}\int_{r-i\infty}^{r+i\infty} A_z^{tot}|_{x=0,y=-\Delta/2}^{x=0,y=\infty} e^{st}ds =$$

$$b\frac{d}{dt}\frac{1}{2\pi i}\int_{r-i\infty}^{r+i\infty}\frac{\mu_0 I}{2\pi}\int_0^\infty \frac{(\xi/\nu)e^{-\zeta d}\,e^{st}}{(s+\alpha)[\zeta cosh(\xi\Delta/2)+(\xi/\nu)sinh(\xi\Delta/2)][\zeta sinh(\xi\Delta/2)+(\xi/\nu)cosh(\xi\Delta/2)]}d\zeta ds \qquad \text{(A2)}$$

First, the total voltage is the sum of the contribution from the source pole, $V_\alpha$, and that from the remaining poles, $V_r$

$$V = V_\alpha + V_r \qquad \text{(A3)}$$

The exact residue expansion for the induced voltage on an optimum coupling loop for $d = 0$ is given in [2]. For $d \neq 0$, the corresponding voltage is contributed to (A3) from the source pole $s = -\alpha$ and the poles given by

$$q_n\,tan(q_n - n\pi/2) = \eta = \frac{1}{2}\nu\zeta\Delta,\ \frac{n\pi}{2} < q_n < \frac{(n+1)\pi}{2}; \qquad \text{(A4)}$$

$$\xi_n = i2q_n/\Delta \qquad \text{(A5)}$$

$$-i\omega_n = s_n = -\frac{4}{\tau_d}(q_n^2 + \zeta^2\Delta^2/4) \qquad \text{(A6)}$$

The contribution from the source pole is

$$V_\alpha = -\alpha b \frac{\mu_0 I}{2\pi}\frac{\nu\Delta}{2} e^{-\alpha t}\left[\int_0^{\frac{\sqrt{\alpha\tau_d}}{\Delta}} \frac{q_\alpha e^{-\zeta d}}{[\eta\cos(q_\alpha)-q_\alpha\sin(q_\alpha)][\eta\sin(q_\alpha)+(q_\alpha)\cos(q_\alpha)]}\,d\zeta + \int_{\frac{\sqrt{\alpha\tau_d}}{\Delta}}^{\infty} \frac{\overline{q_\alpha}\, e^{-\zeta d}}{[\eta\cosh(\overline{q_\alpha})+\overline{q_\alpha}\sinh(\overline{q_\alpha})][\eta\sinh(\overline{q_\alpha})+(\overline{q_\alpha})\cosh(\overline{q_\alpha})]}\,d\zeta\right] \quad \text{(A7)}$$

with

$$q_\alpha = \frac{1}{2}\sqrt{\alpha\tau_d - \zeta^2\Delta^2} \text{ and } \quad q_\alpha = i\,\overline{q_\alpha} \quad \text{(A8)}$$

The remaining voltage contribution from poles given in (A4) is

$$V_r = \sum_{n=0}^{\infty}(-1)^n b \frac{d}{dt}\left[\frac{4\mu_0 I}{\pi\tau_d}\int_{n\pi/2}^{(n+1)\pi/2} \frac{e^{-\zeta d}\, e^{s_n t}}{(s_n+\alpha)} q_n\, dq_n\right] \quad \text{(A9)}$$

or

$$V_r = \sum_{n=0}^{\infty}(-1)^n b \frac{d}{dt}\left[\frac{4\mu_0 I}{\pi}\int_{n\pi/2}^{(n+1)\pi/2} \frac{e^{-\frac{d2q_n}{\Delta\ \nu}tan(q_n-n\pi/2)}\, e^{-\frac{4t}{\tau_d}q_n^2\left[1+\frac{1}{\nu^2}tan(q_n-n\pi/2)\right]}}{\left\{-4q_n^2\left[1+\frac{1}{\nu^2}tan(q_n-n\pi/2)\right]+\alpha\tau_d\right\}} q_n\, dq_n\right] \quad \text{(A10)}$$

The limiting case for $\alpha \to 0$, (A7) does not contribute and thus the total voltage for this case is

$$V = \frac{I}{\Delta\sigma}\frac{b}{\Delta}\sum_{n=0}^{\infty}(-1)^n\left[\frac{4}{\pi\nu}\int_{n\pi/2}^{(n+1)\pi/2} e^{-\frac{d2q_n}{\Delta\ \nu}tan(q_n-n\pi/2)}\, e^{-\frac{4t}{\tau_d}q_n^2\left[1+\frac{1}{\nu^2}tan(q_n-n\pi/2)\right]} q_n\, dq_n\right] \quad \text{(A11)}$$

The limiting case for $\alpha \to \infty\ is$

$$V(\alpha\tau_d) = \sum_{n=0}^{\infty}(-1)^n b \frac{d}{dt}\left[\frac{4\mu_0 I}{\pi}\int_{n\pi/2}^{(n+1)\pi/2} e^{-\frac{d2q_n}{\Delta\ \nu}tan(q_n-n\pi/2)}\, e^{-\frac{4t}{\tau_d}q_n^2\left[1+\frac{1}{\nu^2}tan(q_n-n\pi/2)\right]} q_n\, dq_n\right] \quad \text{(A12)}$$

## Voltage on an Optimum Coupling Loop for $d \to \infty$

For convenience, we evaluate (A2) asymptotically for $d \to \infty$ (resulting in the penetration ratio for $\alpha = 0$ approaches 1 as $t \to \infty$) and therefore the result is not valid for $\alpha = 0$ and $d/\Delta \ll \frac{4t}{\tau_d} \to \infty$. As can be seen from (A11), $V \to 0$ as $t \to \infty$. For $d \neq 0$ case, the $V(t)$ waveform is not very different from that for $d = 0$ [2]. We can use the asymptotic series for the higher order terms and obtain the correction to the leading term and obtain the induced voltage as a function of time. However, because the peak of the induced voltage occurs early in time, typically $\frac{4t}{\tau_d} < 1$ and, at that time, the leading term of the asymptotic expansion for $\alpha = 0$ already approaches the value (A17) for $t \to \infty$. Thus, the peak penetration ratio obtained from the leading term of the expansion is sufficiently accurate.

We seek an asymptotic expansion for (A2) as follows: (1) An integration by parts is used in the ζ-integration with $dU = e^{-\zeta d}d\zeta$ and *W* as the remaining multiplicative factor in (A2). (2) The resulting leading term of the expansion ($\zeta = 0$ and $\xi = \sqrt{s\mu\sigma}$) for $d \to \infty$ is

$$V{\sim}UW|_0^\infty = \frac{I}{\Delta}\frac{b}{d}\frac{1}{\pi}\frac{1}{2\pi i}\int_{r-i\infty}^{r+i\infty}\frac{\sqrt{s\mu\sigma}\Delta e^{st}}{(s+\alpha)sinh(\sqrt{s\mu\sigma}\Delta)}ds = \frac{I}{\Delta}\frac{b}{\pi d}\left[\frac{\sigma\Delta E_z}{H_x}\right]\Big|_{pl} \tag{A13}$$

where (2) is used to replace the inverse Laplace transform by the penetration ratio. The peak induced voltage of (A13) or (7) can thus be expressed in terms of the two multiplicative factors first discussed in the abstract.

Next, how the source pole contribution and the remaining pole contribution behave as $d \to \infty$ is discussed.

First, integrating (A7) by parts gives

$$V_\alpha{\sim}\frac{I}{\Delta\sigma}\frac{b}{\pi d}e^{-\alpha t}\frac{\sqrt{\alpha\tau_d}}{\sin\sqrt{\alpha\tau_d}} \tag{A14}$$

Similarly, the asymptotic limit ($d/\Delta \to \infty$) for the unit step case ($\alpha \to 0$), (A11) can be obtained by integrating by parts as follows:
Let

$$dU = \frac{2}{\nu}[tan(q_n - n\pi/2) + q_n sec^2(q_n - n\pi/2)]e^{-\frac{d2q_n}{\Delta\ \nu}tan(q_n - n\pi/2)}dq_n \tag{A15}$$

and

$$W = \frac{e^{-\frac{4t}{\tau_d}q_n^2\left[1+\frac{1}{\nu^2}tan(q_n - n\pi/2)\right]}_{q_n}}{\frac{2}{\nu}[tan(q_n - n\pi/2)+q_n sec^2(q_n - n\pi/2)]} \tag{A16}$$

Then

$$V = \sum_{n=0}^{\infty}(-1)^n\frac{4b\mu_0 I}{\pi\tau_d}\int_{\frac{n\pi}{2}}^{\frac{(n+1)\pi}{2}} e^{-\frac{d2q_n}{\Delta\ \nu}tan\left(q_n - \frac{n\pi}{2}\right)}\ e^{-\frac{4t}{\tau_d}q_n^2\left[1+\frac{1}{\nu^2}tan\left(q_n - \frac{n\pi}{2}\right)\right]}\ q_n\, dq_n$$

$$\sim \sum_{n=0}^{\infty}(-1)^n\frac{4b\mu_0 I}{\pi\tau_d}UW\Big|_{\frac{n\pi}{2}}^{\frac{(n+1)\pi}{2}} \sim \frac{I}{\sigma\Delta}\frac{b}{\pi d}\sum_{n=0}^{\infty}(-1)^n(2-\delta_{n0})\ e^{-\frac{4t}{\tau_d}\left(\frac{n\pi}{2}\right)^2} \tag{A17}$$

where $\delta_{n0}$ is Kronecker delta ($\delta_{00} = 1$, $\delta_{n0} = 0$ for $n \neq 0$). Equation (A17) agrees with (8) and (2).

The contribution from the remaining poles (A10) for $\alpha \neq 0$ can also be evaluated as

$$V_r = \sum_{n=0}^{\infty}(-1)^n b\frac{d}{dt}\left[\frac{4\mu_0 I}{\pi}\int_{n\pi/2}^{(n+1)\pi/2}\frac{e^{-\frac{d2q_n}{\Delta\ \nu}tan(q_n - n\pi/2)}\ e^{-\frac{4t}{\tau_d}q_n^2\left[1+\frac{1}{\nu^2}tan(q_n - n\pi/2)\right]}}{\left\{-4q_n^2\left[1+\frac{1}{\nu^2}tan(q_n - n\pi/2)\right]+\alpha\tau_d\right\}}q_n\, dq_n\right] \tag{A18}$$

$$V_r = \sum_{n=0}^{\infty}(-1)^n \frac{4b\mu_0 I}{\pi}\frac{d}{dt}\int_{\frac{n\pi}{2}}^{\frac{(n+1)\pi}{2}} \frac{e^{-\frac{d2q_n}{\Delta\ \nu}tan\left(q_n-\frac{n\pi}{2}\right)}\ e^{-\frac{4t}{\tau_d}q_n^2\left[1+\frac{1}{\nu^2}tan\left(q_n-\frac{n\pi}{2}\right)\right]}}{\left\{-4q_n^2\left[1+\frac{1}{\nu^2}tan\left(q_n-\frac{n\pi}{2}\right)\right]+\alpha\tau_d\right\}} q_n\, dq_n\ =$$

$$\frac{d}{dt}\sum_{n=0}^{\infty}(-1)^n \frac{2b\mu_0 I}{\pi}(2-\delta_{n0})\frac{UW}{\left\{-4q_n^2\left[1+\frac{1}{\nu^2}tan\left(q_n-\frac{n\pi}{2}\right)\right]+\alpha\tau_d\right\}}\Bigg|_{\frac{n\pi}{2}}^{\frac{(n+1)\pi}{2}} \quad \text{(A19)}$$

$$V_r \sim \frac{I}{\sigma\Delta}\frac{b}{\pi d}\sum_{n=1}^{\infty}(-1)^n(2-\delta_{n0})\ \frac{(n\pi)^2 e^{-\frac{4t}{\tau_d}\left(\frac{n\pi}{2}\right)^2}}{(n\pi)^2-\alpha\tau_d} \quad \text{(A20)}$$

Equation (A20) with (A14) and (A20) agrees with (7) and (2).

# Appendix B. Voltage on an Optimum Coupling Loop Using an Early-Time Integral

The magnetic vector potential can be simplified as [2], [4]

$$A_z^{tot} \sim \frac{2\mu_0 I}{\pi}\int_1^{\infty}\frac{(\beta^2/\nu)}{\left(\sqrt{\beta^2-1}+\beta/\nu\right)^2\sqrt{\beta^2-1}}\frac{1}{2\pi i}\int_{r-i\infty}^{r+i\infty}\frac{e^{st-F_d(\beta)\sqrt{s\tau_d}}}{S+\alpha}\,ds d\beta \quad \text{(B1)}$$

where $\nu = \frac{\mu}{\mu_0}$ and $F_d(\beta) = \beta + \left(\frac{\rho+d}{\Delta}-1\right)\sqrt{\beta^2-1}$.

Equation (B1) is obtained from (A1) by first taking $cosh\xi\Delta \sim sinh\xi\Delta \sim e^{\xi\Delta}/2$ and $x = 0$ (Figure 4) and then taking the inverse Laplace transform.

For a unit step $\alpha \to 0$ [8],

$$A_z^{tot} \sim \frac{2\mu_0 I}{\pi\alpha}\int_1^{\infty}\frac{(\beta^2/\nu)}{\left(\sqrt{\beta^2-1}+\beta/\nu\right)^2\sqrt{\beta^2-1}}erfc\left[\frac{F_d(\beta)\sqrt{\tau_d}}{2\sqrt{t}}\right]d\beta \quad \text{(B2)}$$

Referring to [2], the magnetic flux passing through the loop in the φ-direction (that is normal to the loop) shown in [4] is calculated below using $\vec{B} = \nabla\times\vec{A}$ in a cylindrical coordinate:

$$B_{\varphi} = -\frac{\partial A_z^{tot}}{\partial\rho};\quad \emptyset > -b\int_{\Delta}^{\infty}\frac{\partial A_z^{tot}}{\partial\rho}d\rho = bA_z^{tot}|_{\rho=\Delta}$$

We can define $V$ as the voltage bound [2] for decaying exponential as

$$V = \frac{\partial\emptyset}{\partial t} = \mu_0 bI\int_1^{\infty}\frac{\beta^2/\nu}{\left(\sqrt{\beta^2-1}+\beta/\nu\right)^2\sqrt{\beta^2-1}}\frac{1}{2\pi i}\int_{r-i\infty}^{r+i\infty}\frac{se^{st-G(\beta)\sqrt{s\tau_d}}}{s+\alpha}\,ds d\beta \quad \text{(B3)}$$

$$G(\beta) = \beta + \frac{d}{\Delta}\sqrt{\beta^2-1} \quad \text{(B4)}$$

$$\frac{V\tau_d}{\mu_0 Ib} \sim \frac{2}{\pi}\left\{\int_1^\infty \frac{(\beta^2/\nu)G(\beta)}{\left(\sqrt{\beta^2-1}+\beta/\nu\right)^2\sqrt{\beta^2-1}} \frac{e^{-[G(\beta)]^2\frac{\tau_d}{4t}}}{2\sqrt{\pi(t/\tau_d)^3}} d\beta - \int_1^\infty \frac{\alpha\tau_d\beta^2/\nu}{\left(\sqrt{\beta^2-1}+\beta/\nu\right)^2\sqrt{\beta^2-1}} e^{-\frac{[G(\beta)]^2\tau_d}{4t}} Re\left[w\left(\sqrt{\alpha t}+\frac{i[G(\beta)]}{2\sqrt{t/\tau_d}}\right)\right] d\beta\right\} \quad \text{(B5)}$$

or

$$\frac{V\tau_d}{\mu_0 Ib} \sim \frac{2}{\pi}\tau_d \frac{d}{dt}\int_1^\infty \frac{\beta^2/\nu}{\left(\sqrt{\beta^2-1}+\beta/\nu\right)^2\sqrt{\beta^2-1}} e^{-\frac{[G(\beta)]^2\tau_d}{4t}} Re\left[w\left(\sqrt{\alpha t}+\frac{i[G(\beta)]}{2\sqrt{t/\tau_d}}\right)\right] d\beta \quad \text{(B6)}$$

For $\alpha\tau_d \to 0$ (the unit step limit),

$$\frac{V\tau_d}{\mu_0 Ib} = \frac{2}{\pi}\int_1^\infty \frac{(\beta^2/\nu)G(\beta)}{\left(\sqrt{\beta^2-1}+\beta/\nu\right)^2\sqrt{\beta^2-1}} \frac{e^{-[G(\beta)]^2\frac{\tau_d}{4t}}}{2\sqrt{\pi(t/\tau_d)^3}} d\beta \quad \text{(B7)}$$

For $\alpha\tau_d \to \infty$ (the impulse limit)

$$\frac{V(\alpha\tau_d)}{\mu_0 Ib} = \frac{2}{\pi}\int_1^\infty \frac{\tau_d\beta^2/\nu}{\left(\sqrt{\beta^2-1}+\beta/\nu\right)^2\sqrt{\beta^2-1}} \frac{1}{2\pi i}\int_{r-i\infty}^{r+i\infty} se^{st-G(\beta)\sqrt{s\tau_d}} ds d\beta,$$

which can be reduced to

$$\frac{V\tau_d(\alpha\tau_d)}{\mu_0 Ib} = \frac{2}{\pi}\int_1^\infty \frac{\frac{\beta^2}{\nu}[G(\beta)]}{\left(\sqrt{\beta^2-1}+\beta/\nu\right)^2\sqrt{\beta^2-1}} \tau_d \frac{d}{dt}\left\{\frac{e^{-[G(\beta)]^2\tau_d/(4t)}}{2\sqrt{\pi(t/\tau_d)^3}}\right\} d\beta \quad \text{(B8)}$$

where

$$\tau_d \frac{d}{dt}\left\{\frac{e^{-[G(\beta)]^2\tau_d/(4t)}}{2\sqrt{\pi(t/\tau_d)^3}}\right\} = e^{-[G(\beta)]^2\tau_d/(4t)}\left\{\frac{[G(\beta)]^2}{8\sqrt{\pi(t/\tau_d)^7}} - \frac{3}{4\sqrt{\pi(t/\tau_d)^5}}\right\} \quad \text{(B9)}$$

In order to take $\alpha\tau_d \to \infty$ of (B6) we use

$$\alpha\tau_d e^{-\frac{[G(\beta)]^2\tau_d}{4t}} Re\left[w\left(\sqrt{\alpha t}+\frac{i[G(\beta)]}{2\sqrt{\frac{t}{\tau_d}}}\right)\right]$$

$$= \alpha\tau_d \frac{1}{2}\left[e^{iG(\beta)\sqrt{\alpha\tau_d}} e^{-\alpha t} erfc\left(i\sqrt{\alpha t}+\frac{G(\beta)\sqrt{\tau_d}}{2\sqrt{t}}\right) + e^{-iG(\beta)\sqrt{\alpha\tau_d}} e^{-\alpha t} erfc\left(-i\sqrt{\alpha t}+\frac{G(\beta)\sqrt{\tau_d}}{2\sqrt{t}}\right)\right]$$

$$\sim \frac{1}{2\sqrt{\pi}} e^{-\frac{[G(\beta)]^2\tau_d}{4t}}\left[\frac{1}{-i\sqrt{\alpha t}+\frac{[G(\beta)]\sqrt{\tau_d}}{2\sqrt{t}}} + \frac{1}{i\sqrt{\alpha t}+\frac{[G(\beta)]\sqrt{\tau_d}}{2\sqrt{t}}}\right] \to \frac{[G(\beta)]}{2\sqrt{\pi(t/\tau_d)^3}} e^{-\frac{[G(\beta)]^2\tau_d}{4t}}$$

Therefore, as $\alpha\tau_d \to \infty$, (B6) becomes (B8).

As $\alpha\tau_d \to 0$, (B6) becomes (B7) because

$$e^{-\frac{[G(\beta)]^2\tau_d}{4t}} Re\left[w\left(\sqrt{\alpha t}+\frac{iG(\beta)}{2\sqrt{\frac{t}{\tau_d}}}\right)\right] \to erfc\left(\frac{G(\beta)\sqrt{\tau_d}}{2\sqrt{t}}\right) \text{ and } \tau_d \frac{d}{dt} erfc\left(\frac{G(\beta)\sqrt{\tau_d}}{2\sqrt{t}}\right) = \frac{G(\beta)}{2\sqrt{\pi(t/\tau_d)^3}}.$$

Letting $u = \sqrt{\beta^2 - 1}$, (B7) ($\alpha \to 0$), becomes

$$\frac{V\tau_d}{\mu_0 Ib} = \frac{2}{\pi}\int_0^\infty \frac{(1+u^2)G(u)/\nu}{\left(u+\sqrt{1+u^2}/\nu\right)^2\sqrt{1+u^2}} \frac{e^{-[G(u)]^2\frac{\tau_d}{4t}}}{2\sqrt{\pi(t/\tau_d)^3}} du \tag{B10}$$

where

$$G(u) = \sqrt{u^2+1} + \frac{d}{\Delta}u \tag{B11}$$

Equation (B8) becomes

$$\frac{V\tau_d(\alpha\tau_d)}{\mu_0 Ib} = \frac{2}{\pi}\int_0^\infty \frac{(1+u^2)G(u)/\nu}{\left(u+\sqrt{1+u^2}/\nu\right)^2\sqrt{1+u^2}} \tau_d \frac{d}{dt}\left\{\frac{e^{-[G(u)]^2\tau_d/(4t)}}{2\sqrt{\pi(t/\tau_d)^3}}\right\} du \tag{B12}$$

Equation (B6) becomes

$$\frac{V\tau_d}{\mu_0 Ib} \sim \frac{2}{\pi}\left\{\tau_d \frac{d}{dt}\int_0^\infty \frac{(1+u^2)/\nu}{\left(u+\sqrt{1+u^2}/\nu\right)^2\sqrt{1+u^2}} e^{-\frac{[G(u)]^2\tau_d}{4t}} Re\left[w\left(\sqrt{\alpha t}+\frac{i[G(u)]}{2\sqrt{t/\tau_d}}\right)\right] du\right\} \tag{B13}$$

## Early-time integral for $d \to \infty$

(B7) can be evaluated for $d \to \infty$ by integration by parts

$$dU = 2\frac{\tau_d}{4t}\left(\frac{u}{\sqrt{u^2+1}}+\frac{d}{\Delta}\right)G(u)e^{-[G(u)]^2\tau_d/(4t)}du\,; \qquad U = e^{-[G(u)]^2\tau_d/(4t)} \tag{B14}$$

$$W = \frac{2}{\pi}\frac{(1+u^2)/\nu}{2\frac{\tau_d}{4t}\left(\frac{u}{\sqrt{u^2+1}}+\frac{d}{\Delta}\right)\left(u+\sqrt{1+u^2}/\nu\right)^2\sqrt{1+u^2}\,2\sqrt{\pi(t/\tau_d)^3}} \tag{B15}$$

$$V = \frac{\mu_0 Ib}{\tau_d}\mathrm{UW}\Big|_0^\infty = \frac{I}{\sigma\Delta}\frac{b}{\pi d}\frac{2}{\sqrt{\pi t/\tau_d}}e^{-\frac{\tau_d}{4t}} \tag{B16}$$

Thus, the voltage on an optimum coupling loop is decomposed into two factors discussed in the abstract. Penetration ratio (A) is $\frac{2}{\sqrt{\pi t/\tau_d}}e^{-\frac{\tau_d}{4t}}$, that is the early-time expansion corresponding to (2) with [1]. Differentiating (B16) with respect to $t/\tau_d$ gives the impulse response ($\alpha \to \infty$):

$$V = \frac{I}{\sigma\Delta}\frac{b}{\pi d}\frac{2}{\sqrt{\pi}}e^{-\frac{\tau_d}{4t}}\left[-\frac{1}{2(t/\tau_d)^{3/2}}+\frac{1}{4(t/\tau_d)^{5/2}}\right] \tag{B17}$$

The unit step early-time peak for the planar penetration ratio $P_p^s$ is found to be $P_p^s/\pi \approx 0.3081$, which is 3.21% lower than the value in Table 1 obtained from (2). On the other hand, the impulse early-time peak for the planar penetration ratio $P_p^i$ agrees with the value obtained from (4) to six digits.

# References


[1]. Johnson, W. A., L. K. Warne, K. C. Chen and E. M. Gurrola, "Linear Diffusion and Internal Voltages in Conducting Enclosures Subjected to a Direct Lightning Strike," Electromagnetics, 15:189-207, 1995.

[2]. Warne, L. K., W. A. Johnson and K. C. Chen, "Maximum Interior Voltage and Magnetic Field Penetration through a Linear Conducting Layer," Journal of Electromagnetic Waves and Applications, Vol. 9, No.4, 1995, pp. 569-598.

[3]. Chen, K. C., Y. T. Lin, L. K. Warne and K. O. Merewether, "Linear diffusion into a Faraday cage," Progress in Electromagnetic Research M, Vol. 23, 299-311, 2012.

[4]. Chen, K. C., Y. T. Lin, L. K. Warne and K. O. Merewether, "Linear Diffusion into a Faraday Cage," SAND2011-8012, *http://prod.sandia.gov/techlib/access-control.cgi/2011/118012.pdf*, December 2011.

[5]. Lee, K. S. H. Editor, **EMP Interaction: Principle, Techniques, and Reference Data**, Revised Printing, Hemisphere Publishing Corporation and Taylor & Francis, 1986 and 1995, pp.559-573.

[6]. Bedrosian, G. and K. H. S. Lee,"EMP Penetration through Metal Skin Panels and Into Aircraft Cavities," AFWL Interaction Note 314, www.ece.unm.edu/summa/notes, August 1976.

[7]. *Lee*, *K.S.H.*, and *G*. *Bedrosian*, "*Diffusive Electromagnetic Penetration into Metallic Enclosures*," *IEEE Transactions* on *Antennas* and *Propagation*, *Vol*. *27*, *No*. *2*, *March 1979*, pp. 194-8.

[8]. M. Abramowitz and I. A. Stegun (editor), **Handbook of Mathematical Functions**, Washington DC: National Bureau of Standards, 1026.